Magnetization reversal in MnAs films: Magnetic force microscopy, SQUID magnetometry, and micromagnetic simulations

R. Engel-Herbert, T. Hesjedal,* J. Mohanty, D. M. Schaadt, and K. H. Ploog
Paul-Drude-Institut für Festkörperelektronik, Hausvogteiplatz 5-7, D-10117 Berlin, Germany
(Received 18 August 2005; revised manuscript received 29 November 2005; published 24 March 2006)

The magnetization reversal of MnAs nanowires was studied by magnetic force microscopy (MFM) imaging in conjunction with superconducting quantum interference device magnetometry and micromagnetic simulations. MnAs films on GaAs(001) exhibit a submicron-sized regular array of ferromagnetic and nonmagnetic stripes, where the width of the stripes can be tuned by the temperature. The investigated thin samples show squarelike hysteresis loops, and the corresponding field-dependent MFM measurements confirm a collective flipping of the domains at the coercive field. Thicker samples, as well as thinner samples at higher temperatures, generally exhibit a rounded magnetization curve with a very low remanent magnetization. Based on three-dimensional micromagnetic simulations, the micromagnetic structure as well as the magnetic hysteresis of MnAs films on GaAs(001) is explained in a consistent way.

DOI: 10.1103/PhysRevB.73.104441 PACS number(s): 75.60.Jk, 75.70.Kw, 68.37.Rt, 76.60.Es

I. INTRODUCTION

Magnetic microstructures and nanostructures offer the opportunity of studying magnetic ordering in the transition regime between atomic and bulk properties.[1] Furthermore, they have unique properties which make them potential candidates for ultrahigh-density storage devices.[2] The study of the magnetic domain configuration and switching mechanism of submicron-sized magnetic elements is a prerequisite for their future technological application in magnetic devices. Among other techniques, magnetic force microscopy (MFM) is widely used for the probing of the magnetic properties of individual nanoparticles[3] and the characterization of the magnetization behavior of coupled ensembles.[4] In single-domain dots the magnetization reversal is well described by the Néel-Brown model of uniform rotation.[5] On the other hand, in the course of the magnetization reversal in magnetic nanowires, the flipping of the magnetization appears to proceed via noncontinuous reversal modes.[6] One possible mechanism is the nucleation of a reversed domain and subsequent domain wall propagation. As the structures become densely packed, the magnetization reversal is also affected by the interparticle interaction. Thus, it is of great importance to study the switching properties of individual, well-separated nanowires as well as their mutual interaction.

MnAs-on-GaAs (001) is a promising ferromagnet-semiconductor hybrid system for spin electronics,[7] as well as magnetologic applications.[8] This system exhibits a regular submicron-sized array of coexisting ferromagnetic and nonmagnetic stripes. Over a wide temperature range, the width of the ferromagnetic stripes can be continuously tuned. The stripe period, on the other hand, is a function of film thickness. This makes MnAs-on-GaAs a unique system for the study of individual, noninteracting nanowires and the coupling between submicron-sized ferromagnetic elements.

The thickness dependence of the integral magnetic properties has been investigated systematically, yielding a saturation magnetization of above 1000 emu/cm^3 for the (nearly) defect-free MnAs film in the α phase.[9] It was found that the magnetization curves measured at room temperature are square like in case of thinner films (<100 nm) and increasingly rounded for thicker films.[9,10] In this paper, we present an investigation of the magnetization reversal in MnAs films on GaAs(001). Field-dependent MFM in combination with superconducting quantum interference device (SQUID) magnetometry was used to observe the reversal process on a microscopic scale.

II. EXPERIMENTAL SECTION

A. Material system MnAs-on-GaAs (001)

Epitaxial MnAs films of high crystal quality have been grown by molecular beam epitaxy (MBE) on the standard semiconductor surfaces of GaAs and Si, as reported in Refs. 11–13. Ferromagnetic α-MnAs exists in the bulk at temperatures below 40 °C and crystallizes in the hexagonal NiAs structure. Above that temperature it transforms into orthorhombic (quasihexagonal) β-MnAs via a first-order phase transition.[14–16] During the coupled structural and magnetic phase transition where the ferromagnetic order breaks down in a discontinuous manner, the lattice spacing of the hexagonal plane (a axis) abruptly shrinks by $\sim$1.0%, whereas along the c axis the lattice spacing remains unchanged. In contrast to this, the phase transition in MnAs films is modified by the epitaxial constraints of the system. In films, the phase transition of MnAs/GaAs(001) no longer proceeds abruptly as in the bulk but a system of alternating α- and β-MnAs stripes extending along the c-axis direction (MnAs[0001]) is stabilized by strain in the broad temperature range from 10 to 40 °C.[17–19] In the α-β-phase coexistence regime, the magnetization decreases continuously as a function of temperature; however, the phase transition itself remains of first order since this can be attributed to the decreasing α-MnAs fraction.[20] The epitaxial relationship and the α-β-stripe structure are illustrated in Fig. 1; for convenience, the surface normal is termed the b axis. The α-β-stripe period p is a linear function of the film thickness t ($p \sim 4.8t$),[9] whereas

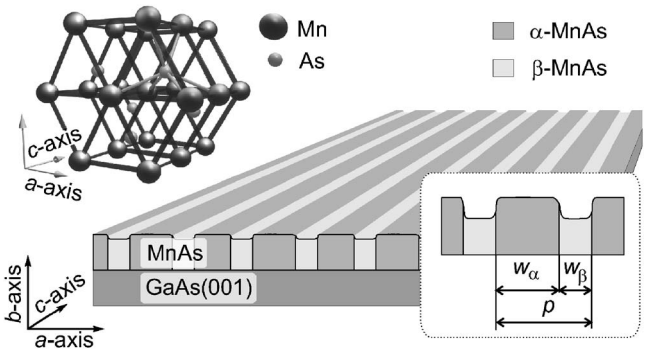

FIG. 1. Sketch of the stripe structure of the strain-stabilized, coexisting α- and β-MnAs phases on GaAs(001) in the temperature range from 10 to 40 °C. In thin films, the in-plane *a* axis is the easy axis of magnetization and the magnetic hard axis is along the *c*-axis direction (MnAs [0001]). A detailed sketch of the hexagonal α -MnAs cell is shown in the upper left-hand side corner.

the α-to-β-phase ratio—and thus the stripe width—is a function of temperature. MnAs exhibits an easy plane of magnetization perpendicular to the *c* axis.[21] In thin MnAs films, the observed magnetic properties are strongly uniaxial with the easy axis along MnAs $[11\bar{2}0]$ (in-plane *a*-axis direction) and the hard axis along the *c*-axis direction; i.e., both easy and hard axes of magnetization lie in the film plane. Applying external magnetic fields in these directions, a 100-nm-thick MnAs film saturates at 100 Oe and 20 kOe, respectively. A field of 10 kOe is necessary to saturate the film normal to the plane due to shape anisotropy.[22]

It has been shown that MnAs grows in two different orientations (*A* and *B* orientations, which are rotated by 90° in the surface plane with respect to each other), depending on the GaAs(001) template.[23] The investigated samples were grown with MnAs in the so-called *A* orientation. However, a small fraction of the 90°-rotated *B* orientation maybe present in the films. The interface formation and layer evolution were examined *in situ* simultaneously by reflection high-energy electron diffraction (RHEED) and reflectance difference spectroscopy. The RHEED intensity corresponding to the *B* orientation decreases with layer thickness and is lost after deposition of 8 nm MnAs.[23] The crystallographic relationship of *A*- and *B*-oriented MnAs is such that the easy axis of magnetization lies in the hard-axis direction of the other phase and vice versa.

B. Magnetic measurements

The variable-field MFM measurements were performed with a commercial MFM (Ref. 24) equipped with a variable-temperature sample holder. A rotatable permanent magnet setup was used to apply the field to the sample.[25] The Cr-Co-coated MFM cantilevers had a spring constant of 0.05 N/m and were magnetized along the tip axis. In this way, the MFM images map the out-of-plane component of the magnetic stray field of the sample. The bright and dark contrast in the MFM images corresponds to a repulsive and an attractive interaction between sample and magnetic tip, respectively. The magnetic hysteresis loops were measured by SQUID magnetometry.[26]

We investigated the domain structure of MnAs at remanence by MFM (Ref. 27) and surface-sensitive x-ray magnetic circular dichroism photoemission electron microscopy (XMCDPEEM).[28] It was observed that the ferromagnetic α-MnAs stripes break up into subdivisions of opposite magnetization along the easy *a* axis, termed (I–III) according to their number.

III. RESULTS

We investigated the magnetization reversal of MnAs thin films on GaAs(001) in the α-β-stripe phase using variable-field MFM. In general, we found two different behaviors in micromagnetic measurements at room temperature. In one case, the film magnetization flips collectively at the coercive field, while in the other case, the film demagnetizes almost completely in the remanent state. To find the origin of this behavior, we further investigated a set of films with different thicknesses with SQUID magnetometry at different temperatures. The obtained hysteresis curves are consistent with the MFM results, exhibiting two different magnetization reversal characteristics: namely, squarelike loops and rounded loops with low remanent magnetization.

A. Magnetization reversal of 140-nm-thick MnAs film

Figure 2(a) shows the hysteresis loop obtained by SQUID magnetometry of an approximately 140-nm-thick MnAs film[29] at 15 °C with the field applied in the easy-axis direction. The hysteresis curve is squarelike with a remanent magnetization close to the saturation magnetization. The ratio of the remanent magnetization to the saturation magnetization is $M_r/M_s=0.99$ and the coercivity is 52 Oe.

A series of MFM images acquired at 15 °C is shown in Fig. 2(b). Squarelike hysteresis loops are commonly observed in thin MnAs films. At 150 Oe, the film is in a single-domain state. The magnetization is along the positive direction of the applied magnetic field. In this case, the MFM response shows neighboring dark and bright stripes, separated by larger gray areas. In Fig. 2(c), a schematic of the stray field (cross section) of fully magnetized stripes is shown (below). The stray field emanates from the sample in the area of the β-MnAs stripes and points into and out of the sample plane at the respective end of the domain. The MFM contrast obtained with a tip magnetized along its axis is bright (dark) in the case of the stray field pointing out of (into) the sample plane, as illustrated above. The position of the ferromagnetic stripes is verified by simultaneously acquired topography scans (not shown). The approximate position of a ferromagnetic stripe segment is indicated by a black rectangle and the magnetization by arrows [cf. measurements ③ and ④, Fig. 2(b)]. At zero applied field, the observed domain structure remains unaffected, which is in accordance with the M_r/M_s ratio of 0.99 observed by SQUID magnetometry. This behavior continues down to almost −50 Oe, where the coercive field is reached and the magnetization reverses collectively. One way of easily iden-

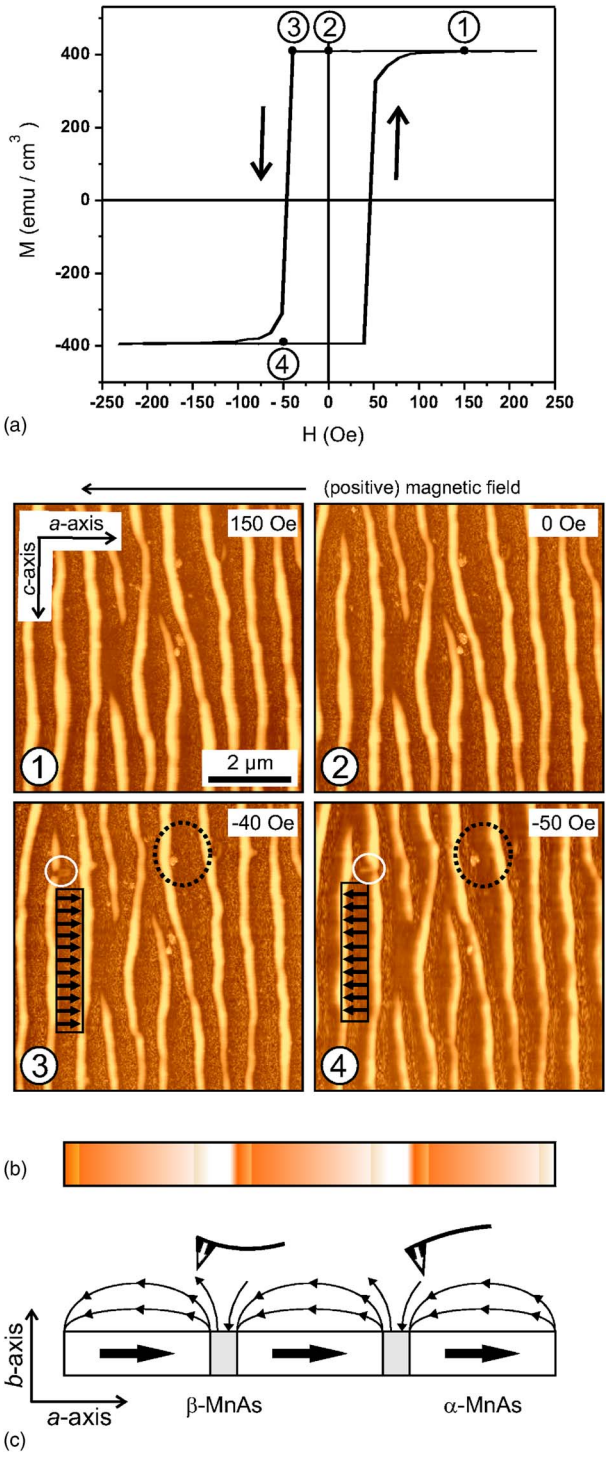

FIG. 2. (Color online) (a) Hysteresis loop measured by SQUID magnetometry with the field applied along the easy *a*-axis direction at 15 °C. The squarelike hysteresis loop exhibits a coercive field of 52 Oe. (b) 7×7 μm^2 MFM scans at 15 °C corresponding to the decreasing field trace. The respective scans are indicated in the magnetization curve. Magnetization reversal occurs by the homogeneous switching of all stripes in the film. The dotted black and white circles mark areas that are reference points described in the text. The arrows in the rectangle indicate the magnetization of the particular stripe. (c) Sketch of the MFM contrast formation (below) and the resulting MFM contrast (above).

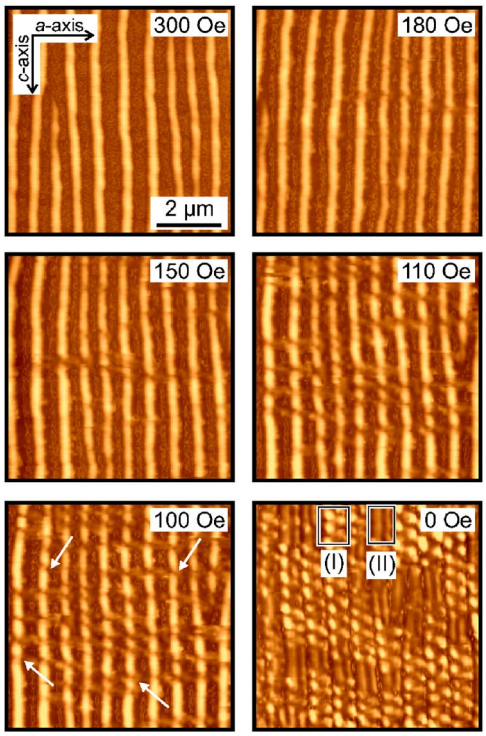

FIG. 3. (Color online) 7×7 μm^2 MFM images of a 180-nm-thick MnAs film, recorded at decreasing applied fields as indicated. At 300 Oe, the sample is fully magnetized. By reducing the applied field below 180 Oe, a continuous decrease of the magnetization aligned in the field direction is observed. From 180 down to 100 Oe, an increasing number of oppositely magnetized domains nucleate; however, no domain wall movement is observed. The domains are correlated across the stripes along the *a*-axis direction. Below 100 Oe, the extended single domains along a stripe decompose into segments of alternatingly magnetized domains. At zero applied field, the sample is almost completely demagnetized.

tifying the collective domain reversal in MFM is the tracking of topographical defects that are also visible as artifacts in the magnetic imaging mode—e.g., indicated by the black circle. Additionally, a pinned domain that has not flipped at −50 Oe is indicated by the white circle.

B. Magnetization reversal of a 180-nm-thick MnAs film

In contrast to the squarelike hysteresis loops observed for the 140-nm-thick film, thicker MnAs films exhibit more rounded hysteresis loops with strongly reduced remanence. To investigate the properties of the rounded hysteresis loops in more detail, we performed MFM measurements of the micromagnetic domain structure on a 180-nm-thick film. Especially, in combination with antiferromagnetic (AFM) and SQUID magnetometry, the possible influences of defects on the hysteresis loop can be studied.

The MFM images presented in Fig. 3 (T=20 °C) are obtained by first fully magnetizing the film. Upon decreasing the applied magnetic field a single-domain state is found (see image at 300 Oe), as observed for the thin film in Fig. 2. The domains start to flip at 180 Oe, leading to a multidomain state. The position of the flipped domains appears to be cor-

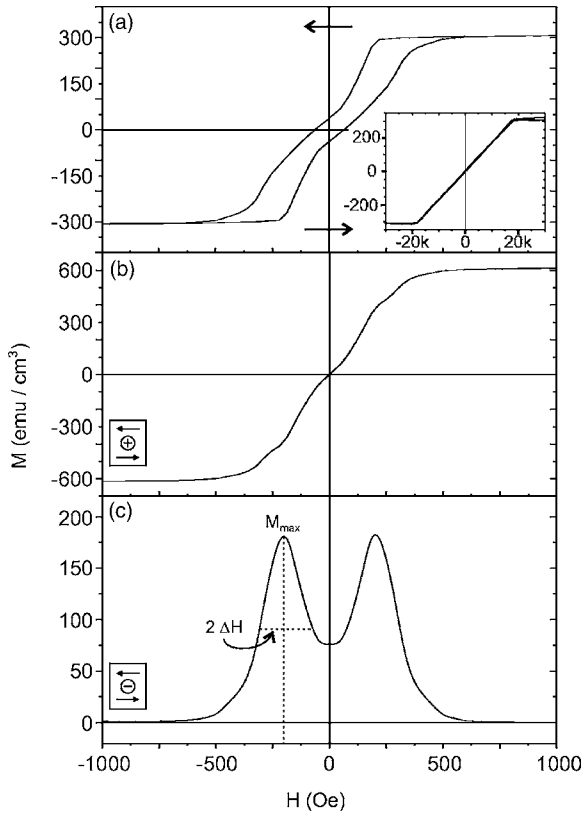

FIG. 4. Hysteresis loop of a 180-nm-thick sample measured at 25 °C with the field applied along the easy axis (a) and at 20 °C with the field applied along the hard axis [see inset in (a)]. The added forward and backward scans (b) and the subtracted traces (c) reveal that the material behaves like a coupled two-phase system with a hard and a soft magnetic component.

related across the stripes (in the *a*-axis direction). The further magnetization-reversal process proceeds via the nucleation of reversed domains rather than domain wall propagation. The flipped domains are also correlated, both in the *a*-axis direction and slightly tilted towards the *c*-axis direction, as indicated in the 100-Oe image. This may have two origins: first, it could be due to the magnetic coupling across the stripes. Second, besides the α-β-stripe structure, additional surface features are found in topography images that exhibit both an *a*-axis-oriented and a slightly tilted step morphology.[30] However, no direct correlation between the *surface* defects and the position of the flipped domains was found.

Below 100 Oe, different domain types appear that all yield a very low net magnetization. On the one hand, alternating sequences of type-I domains along the *c* axis are formed. Type-I domains are single domain across the width of the stripe (along the *a*-axis direction).[27] Alternating sequences of oppositely magnetized type-I domains efficiently demagnetize the stripe as a whole. On the other hand, extended areas of type-II domains appear. Type-II domains are composed of two oppositely magnetized stripe segments along the *a*-axis direction.

Figure 4(a) shows the corresponding hysteresis loop measured at 25 °C. The hysteresis curve is rounded with a very small remanent magnetization $M_r/M_S=0.12$. The coercivity is approximately ±63 Oe. The curve resembles the behavior of a two-phase system consisting of a hard and a soft magnetic contribution.[13] The contribution of the part of the film that has a magnetically hard axis along the field direction can be identified in Fig. 4(b), where the influence of the hysteresis is canceled out by the addition of the forward and backward traces of the hysteresis loop. The curve shows an almost linear behavior, and the magnetization saturates at approximately 600 Oe. The presence of an additional soft-axis loop can be extracted by the subtraction of the forward and backward traces, illustrated in Fig. 4(c). The symmetric two-peak structure shows maxima located at ±190 Oe. From the height of the maxima a remanent magnetization of $M_{\max}/2=92$ emu/cm^3 is obtained and the half width at half maximum leads to a field of $\Delta H \approx 120$ Oe.

C. Thickness dependence of the magnetization reversal

To characterize the different magnetization-reversal regimes in MnAs films, we investigated three film thicknesses at different temperatures in the phase coexistence interval between 10 and 40 °C. The subtraction of the forward and backward branches of the hysteresis curve—i.e., the difference curve—is shown for 140-nm; 180-nm; and 215-nm-thick films in Figs. 5(a)–5(c), respectively. The curve at 15 °C in Fig. 5(a) corresponds to the hysteresis curve presented in Fig. 2(a) and the curve at 25 °C in Fig. 5(b) to Fig. 4.

The 140-nm-thick film shows difference curves from 10 °C to above 30 °C resembling a rectangle function. The rectangular shape is corresponding to an ideal squarelike hysteresis loop; the subtraction of the hysteresis traces leads to a rectangle function centered around zero applied field. The width of the curve is twice the coercive field H_c and the height twice the remanent magnetization M_r. With increasing temperature, M_r decreases because of the temperature-dependent decrease of the ferromagnetic α-phase content. At 30 °C, the curve becomes rounded at zero applied field and a shoulder develops at fields slightly higher than H_c. At this temperature, a transition takes place from the squarelike hysteresis regime to the previously described two-phase characteristics. At 35 °C, the two-phase behavior is fully developed. The 180-nm-thick film tends to the same qualitative behavior; however, the transition takes place between 20 and 25 °C. Furthermore, the offset of the maxima in the two-phase regime increases with increasing temperature. Below the transition temperature, the rectangular curves exhibit a convex decay slightly above the coercive field, whereas the side lobe changes to a concave shape at 20 °C.

The thicker film (215 nm) starts exhibiting the two-phase behavior already at the onset temperature of the α-β-phase coexistence regime of 10 °C. Therefore, Fig. 5(c) also shows measurements at 0 and 5 °C, i.e., fully in the α phase. These two rectangular curves clearly indicate the squarelike loop behavior. The shift of the split maxima is larger than for the 180-nm-thick film at the same temperature. The same observations are made on a large set of samples, reaching from

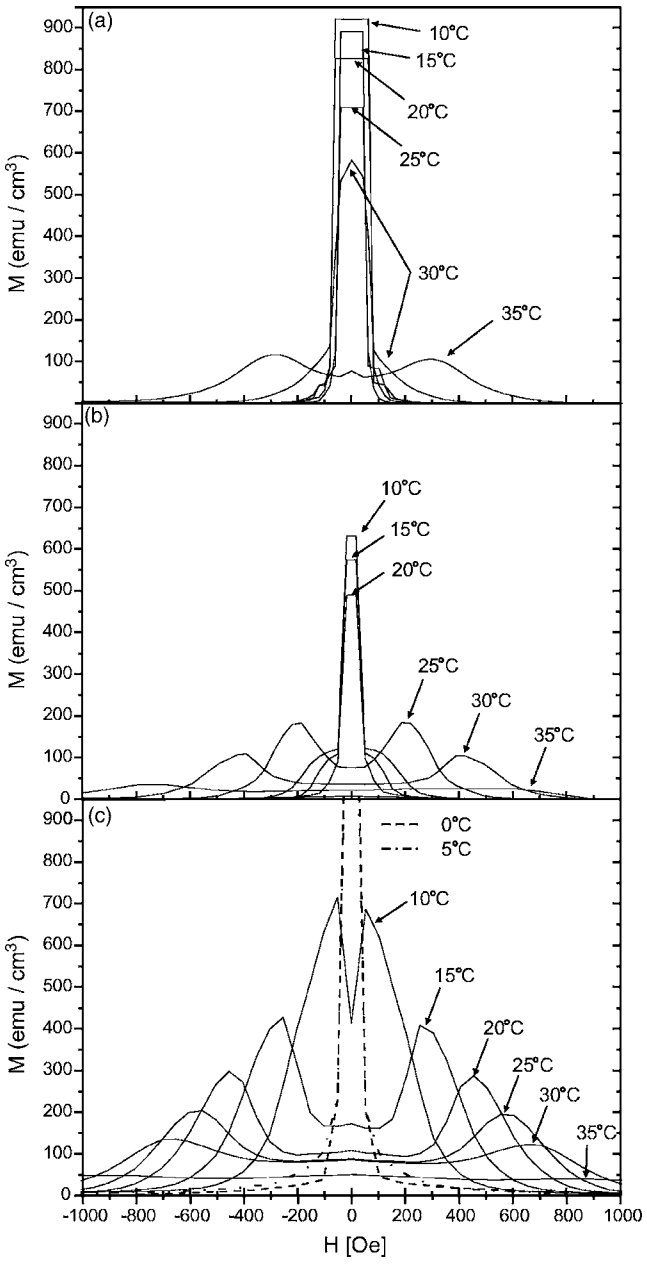

FIG. 5. Subtracted hysteresis curves for (a) 140-, (b) 180-, and (c) 215-nm-thick MnAs film; all three curves are plotted using the same scaling. Independent of film thickness, a double-peak structure is visible at higher temperatures. For lower temperatures, all films exhibit squarelike hysteresis loops resulting in the steplike function centered around zero field. In the case of the 215-nm-thick film, squarelike loops start appearing at the α-β-phase coexistence temperature of 10 °C.

very thin samples (25 nm thick) to samples up to the maximum thickness of 500 nm at which cracking is observed.[9,10]

IV. DISCUSSION

How does magnetization reversal occur in MnAs films on GaAs(001)? The experimental findings can be summarized as follows: a double-peak structure is visible in the difference curves at higher temperatures, independent of film thickness. With increasing film thickness, the two peaks already form at lower temperatures. The offset of the double peaks at a given temperature is larger for thicker films. Two-phase loops are well known for systems composed of a hard and a soft magnetic phase.[31,32] In this system, we observe (i) morphological features which might indicate a magnetically different phase and (ii) different MnAs orientations on GaAs(001). (i) In case of the 180-nm-thick film, the MFM images in Fig. 3 reveal a correlation of the flipped domains across the stripes in the array. The onset of the correlated magnetic features at fields below 180 Oe determines the further nucleation of domains. A similar streaky pattern is also found in topography scans; however, no correlation between topographic and magnetic features was verifiable. (ii) As mentioned above, *A*- and *B*-oriented MnAs are rotated by 90° with respect to each other in the film plane, such that the easy axis of magnetization lies in the hard-axis direction of the other phase. A hysteresis loop in the hard-axis direction of *A*-oriented MnAs, which is a sign of *B*-oriented MnAs in the film, was not found for the investigated samples. Furthermore, one would expect the full saturation of the magnetization along the *a* axis to occur at an applied field of 20 kOe (which is the saturation field of the hard axis), and not at 600 Oe as observed in Fig. 4. As the *B*- to *A*-oriented phase ratio is high for thin films and since phase mixing only occurs at the interfacial area, thin films should exhibit a stronger alteration of the magnetic properties. This means that the *B* orientation is not responsible for the pinning either. Thus, it is worth looking into the peculiarities of the micromagnetic structure of MnAs.

So far, MnAs was treated as a system with an easy-axis in-plane and an out-of-plane intermediate hard axis.[22] The thickness dependence of the observed magnetization-reversal effects makes it necessary to revisit the (micro)magnetic properties of MnAs. In fact, the hexagonal basal plane of MnAs is an easy plane of magnetization since the magnetocrystalline anisotropy constant K_{u1} has a large negative value.[33] Shape anisotropy in thin films selects the in-plane *a* axis as the easy axis of magnetization. As a consequence of the easy-plane property of MnAs, thicker films exhibit truly three-dimensional magnetization patterns, where the domain structure in the easy plane (i.e., *in-depth*) resembles *in-plane* closure domains in patterned permalloy ($Ni_{80}Fe_{20}$) films.[31,34]

Figure 6 shows cross-sectional views in the easy plane of the simulated domain pattern of ferromagnetic α-MnAs stripes. In general, four different remanent magnetization states are found: (a) *S* state, (b) Landau state, (c) diamond state, and a double diamond state (not shown). They give rise to the commonly observed type-I (a), (b) and type-II (c) domains. For the simulation of the magnetization distributions, we assumed the following values for the magnetic parameters of MnAs: saturation magnetization $M_s = 4 \times 10^5$ A/m, exchange stiffness constant $A = 1 \times 10^{-11}$ J/m, and magnetocrystalline anisotropy constants $K_{u1} = -7.2 \times 10^5$ J/m^3 and $K_{u2} = -3.6 \times 10^5$ J/m^3.[35] The dimensions of the simulation grid [(5 nm)^3] were chosen to be as small as the magnetocrystalline and the magnetostatic exchange lengths of $l_{stat} = 5$ nm and $l_{ex} = 5.2$ nm, respectively.[35] The magnetization states are not only a function of the geometrical ratio of the

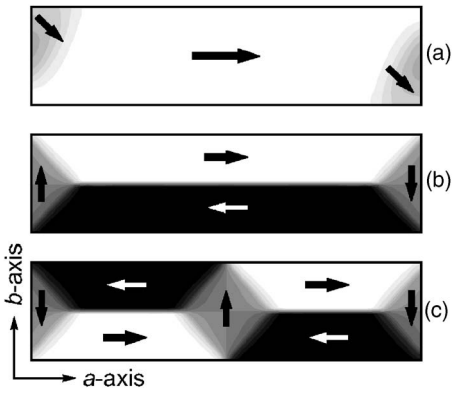

FIG. 6. Magnetization states of MnAs in the easy plane (cross-sectional view *in-depth* cut along the *a*-axis direction): (a) *S* state, (b) Landau state, and (c) diamond state, obtained by three-dimensional micromagnetic simulations. The *S* and the Landau states lead to the observed type-I domains, and the diamond state results in type-II domains. The arrows indicate the magnetization directions.

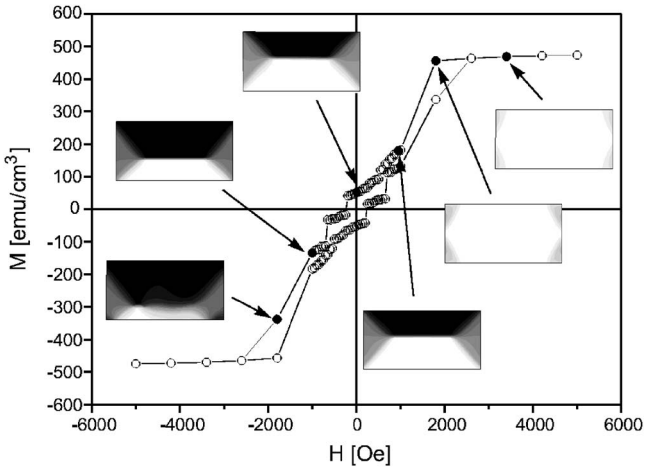

FIG. 7. Simulated hysteresis loop for a 208-nm-thick film showing a Landau state at remanence. The magnetic field is applied along the in-plane *a*-axis direction. The insets show cross-sectional views in the easy plane of the *y* component of the magnetization distribution at the respective field values.

depth over width, which is tuned by temperature, but also of the absolute dimensions, which are given by the thickness of the film. For many combinations of film thickness and temperature, identical geometrical values are obtained. Nevertheless, the micromagnetic structure is distinctly different for thicker films. This is due to the fact that the absolute dimensions are of importance as domain walls are energetically less favored for smaller structures.

Next, we take a look at the magnetization curves resulting from the calculated domain states. The magnetization reversal of an *S* state shown in Fig. 6(a) is well known from calculations of a number of thin film elements, where the *S* state lies in the film plane.[36] The switching occurs in principle between two oppositely magnetized states exhibiting a steep transition in magnetization at the coercive field. The resulting squarelike loop is slightly rounded as a result of the edge domains. This behavior is experimentally found for thin films, as well as for thicker films at low temperatures. For thicker films, the remanent state is most likely a Landau state [Fig. 6(b)] which exhibits a reduced remanent magnetization. In high applied fields, the Landau state transforms into a so-called flower state that is closest to a uniformly magnetized state with deviations from the main magnetization direction at all four edges (cf. upper right-hand-side inset in Fig. 7). Consequently, the hysteresis loop is characterized by the gradual transition from the flower state to the Landau state, resulting in a partial demagnetization of the sample already at large applied fields. For thick films, the remanent state is dominated by the occurrence of a single or double diamond state. Again, at large applied fields, the sample exhibits a flower state. The corresponding hysteresis curve is similar to the result obtained for films with a Landau state at remanence. However, the switching from the flower to the diamond state occurs already at larger applied fields, leading to the observed broadening of the magnetization difference curves [compare Figs. 5(b) and 5(c)].

Figure 7 shows the simulated hysteresis loop of a 208 -nm-thick sample related to the Landau state [Fig. 6(b)]. Magnetization reversal was studied on a sample measuring width (along the *a* axis) $\times$ width (along the *c* axis) $\times$ thickness $=416\times1664\times208$ nm^3 and a cell size of 13 nm. The ratio of width (along the *a* axis) to thickness of 2:1 corresponds to a temperature of approximately 30 °C. The hysteresis curve was calculated starting with a fully magnetized sample at 5000 Oe; the magnetization is pointing in the $+a$ direction. The field was gradually reduced, and the relaxed magnetization distribution was calculated. At selected fields, cross-sectional views of the magnetization distribution in the easy plane are shown. The calculated hysteresis loop is qualitatively in good agreement with the observed curve shown in Fig. 4. As discussed above, the film starts in a flower state at high fields. Upon decreasing the field, the edge domains grow, thereby reducing the magnetization only slightly. Suddenly, at approximately 2000 Oe, the field is small enough for the nucleation of a large, oppositely magnetized domain (cf. cross-sectional view at 1200 Oe). This Landau state is asymmetric—in contrast to the Landau state at remanence. For a lower temperature of approximately 20 °C—i.e., a stripe width (along the *a* axis) of 832 nm—a diamond state is nucleating at lower field, resulting in a narrower magnetization difference curve as the one observed experimentally [cf. Fig. 5(c)].

The numerical simulations lead to a basic understanding of magnetization reversal and the involved processes. Additional simulations reveal that the exact hysteresis curves depend to a large degree on the geometry of the simulated slab, and less on the chosen material parameters. Depending on pinning effects (not related to material inhomogeneities) and the chosen cell size, the coercive field can shift although the overall curve shape remains the same. Due to the uncertainty in the material parameters of MnAs, the exact experimental geometry, and the lack of material inhomogeneities that are responsible for the nucleation process, it is not reasonable to try to reproduce the experimental curve quantitatively. We rather focus on the fact that the simulations reproduce the experimentally observed curves in a qualitative way, independent of the exact simulation parameters.

V. CONCLUSIONS

We have studied the magnetization-reversal process of MnAs films on GaAs(001) by *in situ* variable-magnetic-field MFM, SQUID magnetometry, and micromagnetic simulations. Two distinctively different reversal characteristics were found which occur for certain temperatures and film thicknesses. Supporting micromagnetic simulations reveal that the reason for the different reversal processes lies in the three-dimensional nature of the magnetization distribution—which turns out to be dominant for thick samples and thin stripes due to the altered shape anisotropy. Depending on the dimensions of the ferromagnetic stripes, four different magnetization states were identified in the hexagonal plane. While the *S* state which is characteristic for thin films and wide stripes leads to squarelike hysteresis curves, the Landau state leads to the observed rounded hysteresis curves with low remanent magnetization.

ACKNOWLEDGMENTS

We thank L. Perez for discussions and C. Herrmann for the sample preparation. Part of this work was sponsored by the Bundesministerium für Bildung und Forschung of Germany.

*Present address: Department of Electrical and Computer Engineering, University of Waterloo, Waterloo, Ontario N2L 3G1, Canada. Electronic address: t.hesjedal@ece.uwaterloo.ca

[1] J. Shi, S. Gider, K. Babcock, and D. D. Awschalom, Science **271**, 937 (1996).
[2] J. L. Simonds, Phys. Today **48**(4), 26 (1995).
[3] M. Lederman, S. Schultz, and M. Ozaki, Phys. Rev. Lett. **73**, 1986 (1994).
[4] R. D. Gomez, M. C. Shih, R. M. H. New, R. F. W. Pease, and R. L. White, J. Appl. Phys. **80**, 342 (1996).
[5] W. Wernsdorfer, E. B. Orozco, K. Hasselbach, A. Benoit, B. Barbara, N. Demoncy, A. Loiseau, H. Pascard, and D. Mailly, Phys. Rev. Lett. **78**, 1791 (1997).
[6] R. Ferré, K. Ounadjela, J. M. George, L. Piraux, and S. Dubois, Phys. Rev. B **56**, 14066 (1997).
[7] M. Ramsteiner, H. Y. Hao, A. Kawaharazuka, H. J. Zhu, M. Kästner, R. Hey, L. Däweritz, H. T. Grahn, and K. H. Ploog, Phys. Rev. B **66**, 081304(R) (2002).
[8] C. Pampuch, A. K. Das, A. Ney, L. Däweritz, R. Koch, and K. H. Ploog, Phys. Rev. Lett. **91**, 147203 (2003).
[9] L. Däweritz, L. Wan, B. Jenichen, C. Herrmann, J. Mohanty, A. Trampert, and K. H. Ploog, J. Appl. Phys. **96**, 5056 (2004).
[10] L. Däweritz, C. Herrmann, J. Mohanty, T. Hesjedal, K. H. Ploog, E. Bauer, A. Locatelli, S. Cherifi, R. Belkhou, A. Pavlovska, and S. Heun, J. Vac. Sci. Technol. B **23**, 1759 (2005).
[11] K. Akeura, M. Tanaka, M. Ueki, and T. Nishinaga, Appl. Phys. Lett. **67**, 3349 (1995).
[12] M. Tanaka, J. P. Harbison, M. C. Park, Y. S. Park, T. Shin, and G. M. Rothberg, J. Appl. Phys. **76**, 6278 (1994).
[13] F. Schippan, A. Trampert, L. Däweritz, and K. H. Ploog, J. Vac. Sci. Technol. B **17**, 1716 (1999).
[14] B. T. M. Willis and H. P. Rooksby, Proc. Phys. Soc. London, Sect. B **67**, 290 (1954).
[15] C. P. Bean and D. S. Rodbell, Phys. Rev. **126**, 104 (1962).
[16] R. H. Wilson and J. S. Kasper, Acta Crystallogr. **17**, 95 (1964).
[17] L. Däweritz, F. Schippan, M. Kästner, B. Jenichen, V. M. Kaganer, K. H. Ploog, B. Dennis, K.-U. Neumann, and K. R. A. Ziebeck, *Proceedings of the 28th International Symposium on Compounds and Semiconductors*, IOP Conf. Series No. 170, edited by Y. Arakawa, Y. Hirayama, K. Kishino, and H. Yamaguchi, (IOP, Bristol, 2002), p. 269.
[18] T. Plake, M. Ramsteiner, V. M. Kaganer, B. Jenichen, M. Kästner, L. Däweritz, and K. H. Ploog, Appl. Phys. Lett. **80**, 2523 (2002).
[19] V. M. Kaganer, B. Jenichen, F. Schippan, W. Braun, L. Däweritz, and K. H. Ploog, Phys. Rev. B **66**, 045305 (2002).
[20] A. Ney, T. Hesjedal, C. Pampuch, A. K. Das, L. Däweritz, R. Koch, K. H. Ploog, T. Toliński, J. Lindner, K. Lenz, and K. Baberschke, Phys. Rev. B **69**, 081306(R) (2004).
[21] R. W. De Blois and D. S. Rodbell, Phys. Rev. **130**, 1347 (1963).
[22] F. Schippan, G. Behme, L. Däweritz, K. H. Ploog, B. Dennis, K.-U. Neumann, and K. R. A. Ziebeck, J. Appl. Phys. **88**, 2766 (2000).
[23] F. Schippan, A. Trampert, L. Däweritz, K. H. Ploog, B. Dennis, K. U. Neumann, and K. R. A. Ziebeck, J. Cryst. Growth **201/202**, 674 (1999).
[24] Park Scientific Instruments, Sunnyvale, CA, model M5.
[25] J. Mohanty, R. Engel-Herbert, and T. Hesjedal, Appl. Phys. A: Mater. Sci. Process. **81**, 1359 (2005).
[26] Quantum Design, San Diego, CA, model MPMS.
[27] R. Engel-Herbert, J. Mohanty, A. Ney, T. Hesjedal, L. Däweritz, and K. H. Ploog, Appl. Phys. Lett. **84**, 1132 (2004).
[28] E. Bauer, S. Cherifi, L. Daeweritz, M. Kaestner, S. Heun, and A. Locatelli, J. Vac. Sci. Technol. B **20**, 2539 (2002).
[29] Film thickness determined by cross-sectional scanning electron microscopy.
[30] M. Kästner, C. Herrmann, L. Däweritz, and K. H. Ploog, J. Appl. Phys. **92**, 5711 (2002).
[31] R. Skomski, J. Phys.: Condens. Matter **15**, R841 (2003).
[32] R. Skomski and J. M. D. Coey, Phys. Rev. B **48**, 15812 (1993).
[33] R. W. DeBlois and C. D. Graham Jr., J. Appl. Phys. **29**, 931 (1958).
[34] J. Miltat, G. Albuquerque, and A. Thiaville, *Spin Dynamics in Confined Structures*, chap. 1.
[35] R. Engel-Herbert, T. Hesjedal, and D. M. Schaadt (unpublished).
[36] J.-G. Zhu and Y. Zheng, in *Topics in Applied Physics*, edited by B. Hillebrands and K. Ounadjela (Springer, Berlin, 2002), Vol. 83.